Control of Fano asymmetry in plasmon induced transparency and its application to plasmonic waveguide modulator

Xianji Piao, Sunkyu Yu, and Namkyoo Park*

Photonic Systems Laboratory, School of EECS, Seoul National University, Seoul 151-744, South Korea
*nkpark@snu.ac.kr

Abstract: In this paper, we derive a governing equation for spectral asymmetry in electromagnetically induced transparency (EIT). From the key parameters of asymmetry factor - namely dark mode quality factor Q_d, and frequency separation between bright and dark mode $\Delta\omega_{bd} = (\omega_b - \omega_d)$ -, a logical pathway for the maximization of EIT asymmetry is identified. By taking the plasmonic metal-insulator-metal (MIM) waveguide as a platform, a plasmon-induced transparency (PIT) structure of tunable frequency separation $\Delta\omega_{bd}$ and dark mode quality factor Q_d is suggested and analyzed. Compared to previous works on MIM-based plasmon modulators, an order of increase in the performance Fig. (12dB contrast at ~60% throughput) was achieved from the highly asymmetric, narrowband PIT spectra.

OCIS codes: (250.5300) Photonic integrated circuits; (240.6680) Surface plasmons; (130.3120) Integrated optics devices; (260.2110) Electromagnetic optics.

References and links

1. K. J. Boller, A. Imamolu, and S. E. Harris, "Observation of electromagnetically induced transparency," Phys. Rev. Lett. **66**(20), 2593–2596 (1991).
2. A. André, M. D. Eisaman, R. L. Walsworth, A. S. Zibrov, and M. D. Lukin, "Quantum control of light using electromagnetically induced transparency," J. Phys. At. Mol. Opt. Phys. **38**(9), S589–S604 (2005).
3. A. Kasapi, M. Jain, G. Y. Yin, and S. E. Harris, "Electromagnetically induced transparency: Propagation Dynamics," Phys. Rev. Lett. **74**(13), 2447–2450 (1995).
4. A. H. Safavi-Naeini, T. P. M. Alegre, J. Chan, M. Eichenfield, M. Winger, Q. Lin, J. T. Hill, D. E. Chang, and O. Painter, "Electromagnetically induced transparency and slow light with optomechanics," Nature **472**(7341), 69–73 (2011).
5. S. Zhang, D. A. Genov, Y. Wang, M. Liu, and X. Zhang, "Plasmon-induced transparency in metamaterials," Phys. Rev. Lett. **101**(4), 047401 (2008).
6. N. Liu, L. Langguth, T. Weiss, J. Kästel, M. Fleischhauer, T. Pfau, and H. Giessen, "Plasmonic analogue of electromagnetically induced transparency at the Drude damping limit," Nat. Mater. **8**(9), 758–762 (2009).
7. C. L. Alzar, M. A. G. Martinez, and P. Nussenzveig, "Classical analog of electromagnetically induced transparency," Am. J. Phys. **70**(1), 37–41 (2002).
8. D. D. Smith, H. Chang, K. A. Rosenberger, and R. W. Boyd, "Coupled-resonator-induced transparency," Phys. Rev. A **69**(6), 063804 (2004).
9. M. Tomita, K. Totsuka, R. Hanamura, and T. Matsumoto, "Tunable Fano interference effect in coupled microsphere resonator-induced transparency," J. Opt. Soc. Am. B **26**(4), 813–818 (2009).
10. R. D. Kekatpure, E. S. Barnard, W. Cai, and M. L. Brongersma, "Phase-coupled plasmon-induced transparency," Phys. Rev. Lett. **104**(24), 243902 (2010).
11. Y. Huang, C. Min, and G. Veronis, "Subwavelength slow-light waveguides based on a plasmonic analogue of electromagnetically induced transparency," Appl. Phys. Lett. **99**(14), 143117 (2011).
12. A. E. Çetin, A. Artar, M. Turkmen, A. A. Yanik, and H. Altug, "Plasmon induced transparency in cascaded π-shaped metamaterials," Opt. Express **19**(23), 22607–22618 (2011).
13. P. Tassin, L. Zhang, Th. Koschny, E. N. Economou, and C. M. Soukoulis, "Low-loss metamaterials based on classical electromagnetically induced transparency," Phys. Rev. Lett. **102**(5), 053901 (2009).
14. N. Papasimakis, Y. H. Fu, V. A. Fedotov, S. L. Prosvirnin, D. P. Tsai, and N. I. Zheludev, "Metamaterial with polarization and direction insensitive resonant transmission reponse mimicking electromagnetically induced transparency," Appl. Phys. Lett. **94**(21), 211902 (2009).
15. H. Schmidt, K. L. Campman, A. C. Gossard, and A. Imamoglu, "Tunneling induced transparency: Fano interference in intersubband transitions," Appl. Phys. Lett. **70**(25), 3455–3458 (1997).

#171881 - $15.00 USD Received 5 Jul 2012; revised 24 Jul 2012; accepted 26 Jul 2012; published 2 Aug 2012

16. U. Fano, "Effects of configuration interaction on intensities and phase shifts," Phys. Rev. **124**(6), 1866–1878 (1961).
17. A. E. Miroshnichenko, S. Flach, and Y. Kivshar, "Fano resonances in nanoscale structures," Rev. Mod. Phys. **82**(3), 2257–2298 (2010).
18. V. Giannini, Y. Francescato, H. Amrania, C. C. Phillips, and S. A. Maier, "Fano resonances in nanoscale plasmonic systems: a parameter-free modeling approach," Nano Lett. **11**(7), 2835–2840 (2011).
19. Y. Francescato, V. Giannini, and S. A. Maier, "Plasmonic systems unveiled by Fano resonances," ACS Nano **6**(2), 1830–1838 (2012).
20. F. López-Tejeira, R. Paniagua-Dominguez, R. Rodriguez-Oliveros, and J. Sanchez-Gil, "Fano-like interference of plasmon resonances at a single rod-shaped nanoantenna," New J. Phys. **14**(2), 023035 (2012).
21. C. Argyropoulos, P.-Y. Chen, F. Monticone, G. D'Aguanno, and A. Alù, "Nonlinear plasmonics cloaks to realize giant all-optical scattering switching," Phys. Rev. Lett. **108**(26), 263905 (2012).
22. N. A. Mirin, K. Bao, and P. Nordlander, "Fano resonances in plasmonic nanoparticle aggregates," J. Phys. Chem. A **113**(16), 4028–4034 (2009).
23. C. Min and G. Veronis, "Absorption switches in metal-dielectric-metal plasmonic waveguides," Opt. Express **17**(13), 10757–10766 (2009).
24. W. Cai, J. S. White, and M. L. Brongersma, "Compact, high-speed and power-efficient electrooptic plasmonic modulators," Nano Lett. **9**(12), 4403–4411 (2009).
25. H. A. Haus, *Waves and Fields in Optoelectronics* (Prentice-Hall, New Jersey, 1984).
26. Q. Li, T. Wang, Y. Su, M. Yan, and M. Qiu, "Coupled mode theory analysis of mode-splitting in coupled cavity system," Opt. Express **18**(8), 8367–8382 (2010).
27. P. B. Johnson and R. W. Christy, "Optical constants of the noble metals," Phys. Rev. B **6**(12), 4370–4379 (1972).
28. X. Piao, S. Yu, S. Koo, K. Lee, and N. K. Park, "Fano-type spectral asymmetry and its control for plasmonic metal-insulator-metal stub structures," Opt. Express **19**(11), 10907–10912 (2011).

1. Introduction

Usually manifesting itself in a three-level system, the highly narrow pass-band spectrum of EIT is the result of destructive interference between a bright (broadband) absorption band and a dark (narrowband) resonance state [1]. Supporting a strongly dispersive and narrow pass-band in an opaque medium [2], EIT has been widely studied and used in slow light [3,4] or sensor applications [5,6]. EIT has also been implemented in other platforms, such as electric circuits [7], coupled micro-resonators [8,9], plasmonics, and metamaterial structures [10–14]. EIT being a special case of Fano resonances, its spectrum is in general Fano-asymmetric, as observed in coupled resonators [9], plasmonic systems, metamaterials [10–14], and quantum systems [15]. The Fano asymmetry [16,17], providing a sharp transition in the frequency response, has been a topic of intensive study targeted for frequency-sensitive applications [18–20]. Meanwhile it is well-understood that this spectral asymmetry would compose one of the critical factors in the application of EIT (such as low-power, high-contrast optical switches [21] or sensors [22]), together with the transmittance and bandwidth of the dark mode; nonetheless, most of the prior works have focused only on the realization of EIT in different platforms, setting aside the issue of asymmetry in phenomenological description level.

In this paper, we focus on the control of Fano asymmetry in EIT. By analytically deriving an EIT-asymmetry factor, key routes for the maximization of EIT-asymmetry are identified: use of dark mode having maximum quality factor Q_d, and maximization of the frequency separation $\Delta\omega_{bd} = \omega_b - \omega_d$ between the bright and dark mode. We then suggest one platform of EIT, a stub-pair in the MIM waveguide, supporting a tunable ω_d and a fixed ω_b mode of mutual orthogonality for the maximization of $\Delta\omega_{bd}$. To activate the coupling from bright to the dark mode through quasi-orthogonal mode overlap, symmetry offset in the stub-pair structure is exploited. As a result, highly asymmetric and narrowband PIT spectra are realized, even with the inclusion of metal loss. A study of the structure as a plasmonic waveguide modulator shows performance figures (throughput and modulation depth) at an order higher than previous works [23,24], proving the importance of asymmetry control in EIT applications.

#171881 - $15.00 USD Received 5 Jul 2012; revised 24 Jul 2012; accepted 26 Jul 2012; published 2 Aug 2012

2. Derivation of the spectral asymmetry factor in EIT

Figure 1(a) illustrates the schematic of a generic EIT system, represented with bright-state ($|\psi_b\rangle$) and dark-state ($|\psi_d\rangle$) resonators. Using the coupled mode theory (CMT) and denoting κ_{ib} and κ_{bd} as coupling coefficients between the incident-bright mode and the bright-dark mode respectively, the derivation for the transmittance of the system is straightforward [25,26]. When neglecting the system loss, the transmittance T is expressed as,

$$T = 1 - \frac{1}{1 + [\omega - \omega_b - |\kappa_{bd}|^2 / (\omega - \omega_d)]^2 / \kappa_{ib}} \quad . \tag{1}$$

It is worth mentioning that Eq. (1) is naturally asymmetric in its frequency response, as T is an odd function of $(\omega - \omega_d)$ except for the special case of degeneracy ($\omega_b = \omega_d$). In order to derive an analytical expression for the degree of EIT asymmetry, we examine the generic spectra of the transmittance (Fig. 1(b)) and then define the degree of spectral asymmetry F to be $\Delta\omega_{high} / \Delta\omega_{low}$, the ratio of high / low frequency transmission bandwidths (peak-to-node).

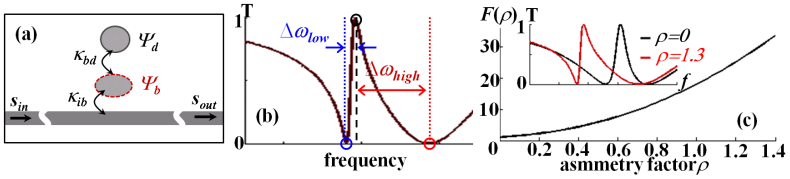

Fig. 1. (a) Schematics of a generic EIT system, represented as coupled dark- and bright-mode resonators. (b) Definition of F (degree of spectral asymmetry) for EIT. (c) behavior of F as a function of the asymmetry factor $\rho = \Delta\omega_{bd} / (2\kappa_{bd})$. Inset shows EIT transmittance at different values of ρ.

By taking the differential $dT/d\omega$ to determine the positions of the transmission peak and nodes, the derivation of F is straightforward. Especially if we introduce a Fano-like asymmetry factor by setting $\rho = (\omega_b - \omega_d)/(2\kappa_{bd})$, F becomes a function of ρ only:

$$F(\rho) = \frac{\sqrt{\rho^2 + 1} + \rho}{\sqrt{\rho^2 + 1} - \rho}. \tag{2}$$

It is critical to mention that since $F(\rho)$ is a monotonic function of ρ (as $dF(\rho)/d\rho > 0$, Fig. 1(c)), an increase of $\rho = \Delta\omega_{bd} / (2\kappa_{bd})$ would equivalently lead to the increase of the EIT asymmetry. Specifically, a maximum asymmetry would be obtained using a dark mode with negligible couplings to incident- or bright-mode ($\kappa_{id} \sim \kappa_{bd} \sim 0$), and by employing at the same time a bright mode having widest bandwidth, as $\max(\Delta\omega_{bd}) \sim \Delta\omega_b / 2$, for ω_d approaching $\omega_b \pm \Delta\omega_b / 2$. For example, a frequency-tunable dark mode (ω_d) of near-zero coupling κ_{bd} to the frequency-fixed widest-bandwidth bright mode (ω_b) could be used for the control or maximization of F. Finally, we note that our definition of the EIT asymmetry factor ρ is in line with the interpretation of the Fano q parameter [16], yet the latter further holds for non-zero coupling κ_{id} between the incident field and discrete mode, unlike the present case of EIT ($\kappa_{id} \sim 0$).

3. Realization of spectral asymmetry in Plasmonic waveguide platform PIT system

For the implementation of the idea, we employ a plasmonic platform on a MIM (Ag-SiO_2-Ag) waveguide. Figure 2(a) shows a MIM stub pair coupled to a waveguide of width w_w composing suggested PIT structure, which provides a bright- and a dark-mode based on the *symmetric*- (Fig. 2(b)) and *anti-symmetric*- (Fig. 2(c)) stub modes, under the y-axis *symmetric* waveguide *incident*-mode excitation. To open a channel of small κ_{bd} between the *bright* (symmetric) and *dark* (anti-symmetric) mode, a perturbation of $\Delta L << L_0$ (L_0: individual stub

#171881 - $15.00 USD Received 5 Jul 2012; revised 24 Jul 2012; accepted 26 Jul 2012; published 2 Aug 2012

length for a symmetric stub-pair) to the symmetric stub-pair is imposed; to make the frequency-split bright modes of $\omega_{b\pm} \sim 1/L_{1\pm}$ ($L_{1\pm} = L_0 \pm \Delta L$) to be quasi-orthogonal ($\kappa_{bd} \neq 0$) to the dark mode of $\omega_d \sim 1/(2L_0 + w_w)$.

Here, it is critical mentioning that the resonant frequency of bright-mode ω_b depends on L_0 and ΔL, while the frequency of dark-mode ω_d is a function of L_0 and waveguide width w_w. Therefore, for a given ΔL, by adjusting w_w it becomes possible to shift ω_d (at fixed ω_b) to achieve the maximization of $\Delta\omega_{bd}$ (and $F(\rho)$). In addition, we also note that the largest κ_{ib} and thus maximum $\Delta\omega_b$ is attained by proactively matching the impedance between the stub and waveguide, with the use of the same waveguide width w_w and stub width w_s ($w_w = w_s = w$). Figure 2(d) shows the plot of $\omega_{b\pm} \sim 1/(L_0 \pm \Delta L)$ (red lines, ΔL = 20nm) and $\omega_d \sim 1/(2L_0 + w)$ (black line; analytic, red circle; COMSOL, *Ag* parameters from [27]) under the control of w (30 ~300nm). With the increase of w, a larger frequency separation $\Delta\omega_{bd}$ is evident. As can be seen from the insets in Fig. 2(d), the strong E_x intensity profile in the junction region for $|\Psi_d\rangle$ again visually explains the dependency in w for the dark mode, in contrast to that of $|\Psi_{b\pm}\rangle$.

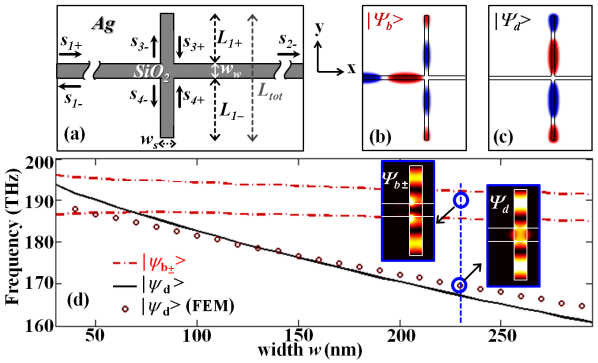

Fig. 2. (a) MIM stub-pair PIT system. Field (H_z) distributions for the (b) symmetric bright mode ($|\Psi_b\rangle$), and (c) anti-symmetric dark mode ($|\Psi_d\rangle$). (d) Resonant frequency of $|\Psi_{b\pm}\rangle$ and $|\Psi_d\rangle$, as a function of w; $\omega_{b\pm} = m{\cdot}c/(n_{eff}{\cdot}L_{1\pm})$ (red lines), and $\omega_d = 2m{\cdot}c/(n_{eff}{\cdot}L_{tot})$ (black line). ΔL fixed at 20nm. $L_0 = m{\cdot}\lambda_{spp}$ (modal number m = 3/4) were used with the effective SPP (surface plasmon polariton) wavelength λ_{spp} calculated from λ_0/n_{eff}, at λ_0 = 1550nm. Insets: E_x intensity profiles for $|\Psi_{b\pm}\rangle$ and $|\Psi_d\rangle$.

Upon identifying key parameters for the maximization of spectral asymmetry and also establishing a PIT platform for its implementation, we now work on the verification of the suggested idea by using both analytic CMT and numerical analysis. For the CMT analysis, we treat the stub-junction region as an ultra-low-Q resonator [28], and write down an equation to represent the interaction between the stub-junction resonator and adjacent waveguides,

$$\frac{da_0}{dt} = (j\omega_0 - \sum_p \frac{1}{\tau_p})a_0 + \sum_p \kappa_p s_{p+} \ , \tag{3}$$

together with equations for energy conservation [28]

$$s_{p-} = -s_{p+} + \kappa_p^* a_0 \ , \tag{4}$$

where $s_{p\pm}$ is the field amplitude in waveguide p = 1 ~4, coupling into (+) or out of (-) the resonator (of field amplitude a_0 and resonant frequency ω_0), and κ_p (= $(2/\tau_p)^{1/2}$ [28]) is the coupling coefficient between the junction resonator and adjacent waveguides.

By noting that the dark-mode $|\Psi_d\rangle$ extending over waveguides 3 *and* 4 couples to bright modes $|\Psi_{b+}\rangle$ and $|\Psi_{b-}\rangle$ solely occupying waveguides 3 and 4 respectively, we write:

$$\frac{da_d}{dt} = (j\omega_d - \frac{1}{\tau_{d3}} - \frac{1}{\tau_{d4}})a_d + \kappa_{bd3}s_{3-} + \kappa_{bd4}s_{4-} \ , \ and \tag{5}$$

#171881 - $15.00 USD Received 5 Jul 2012; revised 24 Jul 2012; accepted 26 Jul 2012; published 2 Aug 2012

$$s_{3,4+} = (s_{3,4-} - \kappa^*_{bd\,3,4}\, a_d)\cdot e^{-j\varphi_{3,4}}\,, \qquad (6)$$

where $\phi_p = 2\pi\cdot(2L_p/\lambda_{spp})$, $\lambda_{spp} = \lambda_0/n_{eff}$; and $\kappa_{bd3(4)}$ is the coupling coefficient between the dark mode resonator (of field amplitude a_d and resonant frequency ω_d) and the field $s_{3(4)-}$, coupling from the junction region into the dark mode resonator residing in the stub region.

Solving Eqs. (3) ~(6) for s_{3+} and s_{4+}, and then applying boundary conditions of $s_{1+} = 1$ and $s_{2+} = 0$ with first-order approximations of $\tau_1 \sim\tau_2 \sim\tau_3 \sim\tau_4 \sim\tau_0 \sim 0$ (for ultra-low Q junction resonator) and $\tau_{d3} \sim\tau_{d4} \sim\tau_d$ ($\Delta L << L_0$) we get:

$$s_{p(q)+} = \frac{(j(\omega-\omega_0)-2/\tau_d)(e^{j\varphi_q}+1)}{(j(\omega-\omega_0)+2/\tau_d)\cdot(e^{j\varphi_p}+e^{j\varphi_q}+2e^{j(\varphi_p+\varphi_q)})},\ for\ \ p=3(4)\ and\ \ q=4(3)\,. \qquad (7)$$

Now using $t = s_{2-}/s_{1+} = s_2$ ($s_{1+} = 1$) and since $s_{2-} = \kappa^* a_0$, by expressing a_0 in terms of s_{3+} and s_{4+} using Eq. (3) we finally arrive at the PIT transmittance T of the system:

$$t = \kappa^* a_0 = \kappa^* \frac{\sum_p \kappa_p s_{p+}}{j(\omega-\omega_0)+\sum_p 1/\tau_p} \cong \frac{2/\tau_0 (s_{1+}+s_{2+}+s_{3+}+s_{4+})}{j(\omega-\omega_0)+4/\tau_0} \cong \frac{1+s_{3+}+s_{4+}}{2}\,, \qquad (8)$$

$$T = |t|^2 = \left|\frac{jA_d(e^{j\varphi_3}+e^{j\varphi_4}+e^{j(\varphi_3+\varphi_4)}+1)+e^{j(\varphi_3+\varphi_4)}-1}{(jA_d+1)(e^{j\varphi_3}+e^{j\varphi_4}+2e^{j(\varphi_3+\varphi_4)})}\right|^2,\ \ where\ \ A_d = (\omega-\omega_d)\cdot\tau_d/2\,. \qquad (9)$$

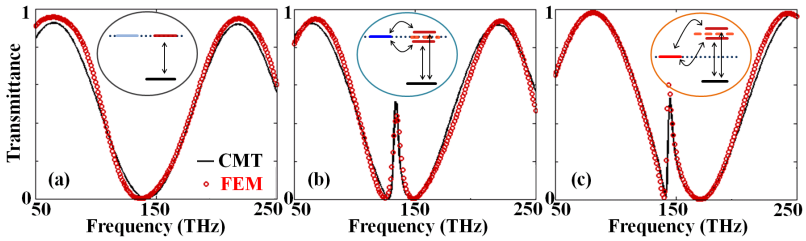

Fig. 3. Transmittance spectra from CMT (lines) and COMSOL (circles), for stub pair - waveguide PIT structures of; (a) $\Delta L = 0$ and $w = 40$nm, (b) $\Delta L = 20$nm and $w = 40$nm (c) $\Delta L = 20$nm and $w = 80$nm. $L_\pm = 5/4\lambda_{spp} \pm \Delta L$. Insets show relative energy levels of $|\Psi_{b\pm}>$ and $|\Psi_d>$ for each structure.

The black lines in Fig. 3 show the plot of the transmittance T using the CMT result of (9). It is worth noting that the metallic loss of Ag has been incorporated in the equation through the phase evolution terms $\phi_p = 2\pi\, n_{eff}\cdot(2L_p/\lambda_0)$, with n_{eff} extracted from the MIM waveguide analysis using COMSOL. A perfect fit in the PIT spectra between the CMT and numerical (COMSOL) results have been achieved, by using two fitting parameters of ω_d and τ_d obtained from the numerical result. As expected, without a perturbation to the structural symmetry (i.e., case of $\Delta L = 0$, Fig. 3(a)), the dark mode excitation is inhibited (as $\kappa_{bd} = 0$). In contrast, with a perturbation of $\Delta L = 20$nm (Fig. 3(b) and 3(c)) to the symmetric stub-pair, the excitation of the dark mode is evident. Finally, with the increase of the MIM waveguide width w (40nm and 80nm for Fig. 3(b) and 3(c) respectively), dramatic changes in the PIT-asymmetry $\rho \sim\omega_b - \omega_d(w)$ were observed, as expected. It is worth mentioning that by employing a higher refractive index material in the waveguide-stub junction region to increase the *effective* junction width w_{eff}, it was possible to obtain equivalent results.

4. Optimization of the structure and application to an MIM plasmonic modulator

Utilizing the steeper side of asymmetric PIT spectra, we now study the performance of our structure as an MIM waveguide plasmonic modulator (inset in Fig. 4(a)), by using a voltage-controlled electro-optic polymer in the waveguide for the shift of the PIT transmission peak

#171881 - $15.00 USD Received 5 Jul 2012; revised 24 Jul 2012; accepted 26 Jul 2012; published 2 Aug 2012

(dashed line in Fig. 4(a), for 2V bias. Δn = 0.008 [24]). Under the application of bias, the switching action of the modulator is evident from Fig. 4(b) (on-state) and Fig. 4(c) (off-state).

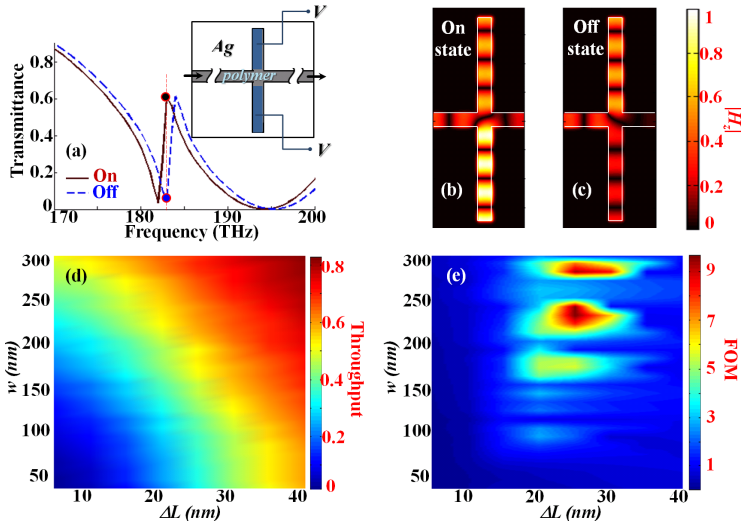

Fig. 4. (a) Transmittance spectra from the modulator in on (black, V = 0) and off (blue, V = 2) states. The inset shows the structure of the modulator. The refractive index of electro-optic polymer in the stub region can be controlled with the overlaid electrodes [24]. Magnetic field amplitude distribution of the modulator in on (b), and off (c) states (w = 230nm, ΔL = 25nm, ΔV = 2). (d) Throughput and (e) FOM of the modulator as a function of w (30 ~300nm) and ΔL (5 ~40nm). Media 1 and Media 2 are provided for b, c respectively.

Defining the figure of merit (FOM) of the modulator as T/M (T = throughput, M = modulation depth = T_{off} / T_{on}), the parameter scanning for an optimal stub-waveguide structure has been carried out. Figures 4(d) and 4(e) show Throughput and FOM of the modulator plotted as a function of w and ΔL. An impressive FOM value of 9.5 was achieved with excellent throughput (M = – 12.3dB, T = 60%) with the parameter set of w = 230nm and ΔL = 25nm; which is an order higher than the previous record of FOM = 1 (M = – 3dB, T = 50%) [24].

5. Conclusion

We demonstrated the control and maximization of spectral asymmetry in EIT, through the tuning of key parameters obtained from the analytically derived asymmetry factor. For the real implementation, we proposed an MIM-waveguide-coupled symmetric stub pair, with a perturbation of its spatial symmetry. Application to a plasmonic waveguide modulator showed an order of improvement in its figure of merit when compared to previous records, proving the importance of asymmetry control in the EIT spectrum. We note that our general CMT derivation of EIT asymmetry factor ρ and consequent findings should be applicable to other platforms of EIT or EITs of multiple dark modes – not limited to plasmonics – for the purpose of designing devices which require extremely narrowband and asymmetric spectra, such as low-power high-contrast switches, high-sensitivity sensors, or slow-light based optical buffers.

Acknowledgments

This work was supported by the National Research Foundation; GRL, K20815000003, Global Frontier Program 2011-0031561, and Center for Subwavelength Optics, SRC 2012-0000606, all funded by the Korean government.

#171881 - $15.00 USD Received 5 Jul 2012; revised 24 Jul 2012; accepted 26 Jul 2012; published 2 Aug 2012